Meccanica (2016) 51:2185–2201
DOI 10.1007/s11012-015-0348-0

Thermal buckling of temperature dependent FG-CNT reinforced composite plates

M. Mirzaei · Y. Kiani

Received: 1 September 2015 / Accepted: 10 December 2015 / Published online: 17 December 2015

Abstract Thermally induced bifurcation buckling of rectangular composite plates reinforced with single walled carbon nanotubes is investigated in this research. Distribution of CNTs across the thickness of the plate is considered to be uniform or functionally graded. Thermomechanical properties of the constituents are considered to be temperature dependent. Equivalent properties of the composite media are obtained by means of a modified rule of mixtures approach. First order shear deformation plate theory is used to formulate the governing equations. An energy based Ritz method is used to obtain the algebraic presentation of the stability equations. Due to their fast convergence feature, Chebyshev polynomials are adopted as the basis of the shape functions. Various combinations of clamped, simply supported, sliding supported and free boundary conditions with normal to edge immovable or movable features are considered. An iterative process is applied to obtain the critical buckling temperature of composite plates with temperature dependent material properties. Numerical result are given to explore the influences of various parameters such as characteristics of CNTs, geometrical characteristics of the plate and boundary conditions. It is shown that, in most of the cases, FG-X pattern of the CNTs is the most influential case since it results in higher critical buckling temperatures.

Keywords Thermal buckling · Carbon nanotube reinforced composite · Chebyshev–Ritz method · Rectangular plate

1 Introduction

In classical thin solid structures, such as beams, plates and shells, studying the buckling phenomenon is of high interest. Similar to mechanical buckling, thermal stresses may result in buckling when certain conditions are met for boundary conditions and types of thermal stresses. With the introduction of novel types of materials, such as functionally graded materials (FGM) or carbon nanotubes (CNTs), recent researches of investigators are focused on these classes of materials.

Thermal stability of functionally graded material plates is well-documented in the open literature in the past decade. Some authors investigated the linear thermal buckling response of functionally graded material plates [1–5] and some others used a completely nonlinear analysis to obtained the critical buckling temperature as well as post-buckling equilibrium paths of the plate [6–12].

Carbon nanotubes (CNTs) have exceptional thermomechanical properties which made them as a

M. Mirzaei
Department of Mechanical Engineering, Faculty of Engineering, University of Qom, Qom, Iran

Y. Kiani (✉)
Mechanical Engineering Department, Amirkabir University of Technology, Tehran, Iran
e-mail: y.kiani@aut.ac.ir

candidate for reinforcement of the composites [13]. It is reported that nonuniform distribution of CNTs may be achieved through a powder metallurgy process [14]. Therefore the concept of FGMs and CNTs may be achieved together through a nonuniform distribution of CNTs through a specific direction [15]. This class of materials are known as functionally graded carbon nanotube reinforced composites (FG-CNTRC).

Uniaxial and biaxial buckling of composite plates reinforced with single walled carbon nanotubes is reported by Jafari et al. [16]. Ehselby-Mori-Tanaka and modified rule of mixtures approaches are used to estimate the properties of the nanocomposite media. Solution of this research is suitable only for plates with all edge simply supported. Exact closed form expressions are provided through the Navier solution method. Mechanical buckling response of FG-CNTRC composite plates with various boundary conditions and subject to various combinations of compression/tension loads is investigated by Lei et al. [17]. Solution of this method is based on an element-free kp-Ritz method. Since nonsymmetric distribution of CNTs across the thickness of the plate results in nonlinear bending rather than the buckling/postbuckling problem, only symmetric distributions of CNTs across the plate thickness are considered. Zhang et al. [18] studied the buckling response of FG-CNTRC plates resting on the Winkler elastic foundation. Elastic foundation is of conventional type which acts in compression as well as in tension. First order plate theory is used to obtain the governing stability equations. Similar to the investigation of Lei et al. [17], uniaxial compression, biaxial compression and combined compression/tension types of buckling are considered in this research. Material properties of the composite media are obtained according to a modified rule of mixtures approach. In two other studies, Lei et al. [19] and Zhang et al. [20] investigated the buckling behaviour of moderately thick skew plates with or without contact with elastic foundation using mesh-free methods based on a first order shear deformation theory. For the case of an FG-CNTRC plate integrated with two identical piezoelectric layers, Wu and Chang [21] studied the bifurcation buckling based on Reissner's mixed variational theorem. In this study, three dimensional elasticity formulation is used rather than a two dimensional lumped plate theory formulation. Plate is subjected to in-plane biaxial compression and finite element method is used to solve the stability equations.

Shen and Zhu [22] investigated the buckling and post-buckling responses of sandwich plates with CNTRC face sheets in thermal environment. It is shown that characteristics of CNTs in face sheets are influential on buckling and post-buckling features of the sandwich plate. Shen and Zhang [23] studied the thermal buckling and postbuckling of FG-CNTRC rectangular plates with symmetric distribution of CNTs across the plate thickness. It is reported that, plates with intermediate volume fraction of CNTs have not, necessarily, intermediate critical buckling temperatures. Zhang et al. [24], also, studies the post-buckling of FG-CNTRC rectangular plates with edges elastically restrained against translation and rotation under the von-Kármán plate assumptions. Rafiee et al. [25] proposed a closed form solution for thermal postbuckling of rectangular plates made of FG-CNTRC plates integrated with smart piezoelectric layers with all edges simply supported.

Similar to stability analysis of FG-CNTRC plates, many studies are available on geometrically nonlinear static response [26–29], vibrational behaviour [30–36], dynamic response [37] and dynamic stability [38] of plates made from FG-CNTRC.

As the above literature survey reveals, while the literature is wealth enough on the subject of mechanical stability of FG-CNTRC plates, the only available works on the subject of thermal stability of FG-CNTRC plates belong to Shen and Zhang [23] and Rafiee et al. [25]. The above-mentioned researches, however, are confined to the case of plates with all edges simply supported. Present investigation aims to analyze the thermal buckling response of FG-NCTRC plate subjected to uniaixal or biaxial in-plane thermal loading via a Ritz formulation which is valid for arbitrary types of in-plane/out-of-plane boundary conditions. First order plate theory is used to obtain the governing equations of the plate. Material properties of the matrix and reinforcements are assumed to be linearly thermoelastic. Chebyshev polynomials are used as the basis shape functions suitable for arbitrary boundary conditions such as simply supported, clamped, free and sliding supported. An eigenvalue problem is established to obtain the critical buckling temperatures of temperature dependent rectangular FG-CNTRC plates. After performing the comparison studies to assure the effectiveness and correctness of

the proposed formulation and solution method, parametric studies are given to explore the influences of various involved parameters such as volume fraction and dispersion profile of CNTs, geometrical properties of the plate and boundary conditions. It is shown that, all of the above-mentioned parameters are influential on buckling temperature and buckled shapes of the plate. Especially the FG-X pattern results in higher critical buckling temperature and is more suitable for thermal stability resistance.

2 Basic formulation

An FG-CNTRC rectangular plate is considered is this research. Thickness, width and length of the plate are denoted by, h, b and a, respectively. The conventional Cartesian coordinate system with its origin located at the center of the plate where $-0.5a \leq x \leq +0.5a$, $-0.5b \leq y \leq +0.5b$, and $-0.5h \leq z \leq +0.5h$ is considered.

Plate is made from a polymeric matrix reinforced with single walled carbon nanotube (SWCNT). Distribution of SWCNT across the plate thickness may be uniform (referred to as UD) or functionally graded (referred to as FG) [26, 30–32, 39, 40]. In this research, three types of FG distribution of CNTs and the UD case are considered. FG-V, FG-O and FG-X CNTRC are the functionally graded distribution of carbon nanotubes through the thickness direction of the rectangular composite plate.

Generally, the effective thermo-mechanical properties of the FG-CNTRC rectangular plate are obtained using the well-known homogenization schemes, such as Mori-Tanaka scheme[41] or the rule of mixtures [42]. For the sake of simplicity, in the present research, the rule of mixtures is used to obtain the properties of the composite plate. However to account for the scale dependent properties of nanocomposite media, efficiency parameters are introduced. Accordingly, the effective material properties may be written as [43–47]

$$\begin{aligned} E_{11} &= \eta_1 V_{CN} E_{11}^{CN} + V_m E^m \\ \frac{\eta_2}{E_{22}} &= \frac{V_{CN}}{E_{22}^{CN}} + \frac{V_m}{E^m} \\ \frac{\eta_3}{G_{12}} &= \frac{V_{CN}}{G_{12}^{CN}} + \frac{V_m}{G^m} \end{aligned} \tag{1}$$

In the above equations, η_1, η_2 and η_3 are the so called efficiency parameters and as mentioned earlier are introduced to account for the size dependent material properties of the plate. These constants are chosen to equal the obtained values of Young modulus and shear modulus from the present modified rule of mixtures with the results obtained according to the molecular dynamics simulations [43]. Besides, E_{11}^{CN}, E_{22}^{CN} and G_{12}^{CN} are the Young's modulus and shear modulus of SWCNTs, respectively. Furthermore, E^m and G^m indicate the corresponding properties of the isotropic matrix.

In Eq. (1), volume fraction of CNTs and matrix are denoted by V_{CN} and V_m, respectively which satisfy the condition

$$V_{CN} + V_m = 1 \tag{2}$$

As mentioned earlier, three types of functionally graded CNTRC plates are considered. These types along with the UD type are the considered patterns of CNT dispersion through the thickness of the plate. In Table 1 distribution function of CNTs across the plate thickness is provided.

It is easy to check from Table 1 that, all of these types have the same value of volume fraction. The total volume fraction across the plate thickness in all of these cases is equal to V_{CN}^*. In FG-X type distribution of CNT is maximum near the top and bottom surfaces whereas the mid-plane is free of CNT. For FG-O, however, top and bottom surfaces are free of CNTs and the mid-surface of the plate is enriched with CNTs. In FG-V, the top surface is enriched with CNT and the bottom one is free of CNT. In UD type, each surface of the plate though the thickness has the same volume fraction of CNTs.

The effective Poisson ratio depends weakly on position [43, 44] and is expressed as

$$v_{12} = V_{CN}^* v_{12}^{CN} + V_m v^m \tag{3}$$

Table 1 Volume fraction of CNTs as a function of thickness coordinate for various cases of CNTs distribution

CNTs distribution	V_{CN}
UD CNTRC	V_{CN}^*
FG-V CNTRC	$V_{CN}^*\left(1+2\frac{z}{h}\right)$
FG-O CNTRC	$2V_{CN}^*\left(1-2\frac{\lvert z\rvert}{h}\right)$
FG-X CNTRC	$4V_{CN}^*\frac{\lvert z\rvert}{h}$

Following the Shapery model, longitudinal and transverse thermal expansion coefficients are expressed as [43]

$$\alpha_{11} = \frac{V_{CN}E_{11}^{CN}\alpha_{11}^{CN} + V_m E^m \alpha^m}{V_{CN}E_{11}^{CN} + V_m E^m}$$
$$\alpha_{22} = \left(1 + \nu_{12}^{CN}\right)V_{CN}\alpha_{22}^{CN} + (1 + \nu^m)V_m\alpha^m - \nu_{12}\alpha_{11} \tag{4}$$

where in the above equation, α_{11}^{CN}, α_{22}^{CN} and α^m are the thermal expansion coefficients of the constituents.

First order shear deformation theory (FSDT) of plates suitable for moderately thick and thick plates is used in this study to estimate the kinematics of the plate [48]. According to the FSDT, displacement components of the plate may be written in terms of characteristics of the mid-surface of the plate and cross section rotations as

$$\begin{aligned} u(x,y,z) &= u_0(x,y) + z\varphi_x(x,y) \\ v(x,y,z) &= v_0(x,y) + z\varphi_y(x,y) \\ w(x,y,z) &= w_0(x,y) \end{aligned} \tag{5}$$

In the above equation u, v, and w are the through-the-length, through-the-width and through-the-thickness displacements, respectively. Mid-plane characteristics of the plate are designated with a subscript 0. Besides, transverse normal rotations about the x and y axes are denoted by φ_y and φ_x, respectively.

According to FSDT, in-plane strain components are written in terms of mid-plane strains and change in curvatures. Besides, through-the-thickness shear strain components are assumed to be constant. Therefore, one may write

$$\begin{Bmatrix} \varepsilon_{xx} \\ \varepsilon_{yy} \\ \gamma_{xy} \\ \gamma_{xz} \\ \gamma_{yz} \end{Bmatrix} = \begin{Bmatrix} \varepsilon_{xx0} \\ \varepsilon_{yy0} \\ \gamma_{xy0} \\ \gamma_{xz0} \\ \gamma_{yz0} \end{Bmatrix} + z\begin{Bmatrix} \kappa_{xx} \\ \kappa_{yy} \\ \kappa_{xy} \\ \kappa_{xz} \\ \kappa_{yz} \end{Bmatrix} \tag{6}$$

In this study, a rectangular plate under the action of uniform heating is under investigation. At least on two parallel edges of the plate normal to edge displacements are restrained. Under such conditions, the plate cannot go thermal expansion at least along one direction and compressive thermal stresses are induced. Therefore, buckling phenomenon may happen. It is known that buckling is a nonlinear phenomenon which should be obtained under geometrically nonlinear analysis. Meanwhile, when only bifurcation buckling is of interest, stability equations are linearised. Therefore, to obtain the stability equations associated with the onset of buckling, strain components may be assumed to be infinitesimal and therefore linear strain-displacement relations suffice. In such solution method, the potential energy due to the prebuckling forces should be included as is shown in the next.

Considering the above mentioned discussions, the components of the strain associated to the mid-surface of the plate are linearised and are equal to

$$\begin{Bmatrix} \varepsilon_{xx0} \\ \varepsilon_{yy0} \\ \gamma_{xy0} \\ \gamma_{xz0} \\ \gamma_{yz0} \end{Bmatrix} = \begin{Bmatrix} u_{0,x} \\ v_{0,y} \\ u_{0,y} + v_{0,x} \\ \varphi_x + w_{0,x} \\ \varphi_y + w_{0,y} \end{Bmatrix} \tag{7}$$

and the components of change in curvature compatible with the FSDT are

$$\begin{Bmatrix} \kappa_{xx} \\ \kappa_{yy} \\ \kappa_{xy} \\ \kappa_{xz} \\ \kappa_{yz} \end{Bmatrix} = \begin{Bmatrix} \varphi_{x,x} \\ \varphi_{y,y} \\ \varphi_{x,y} + \varphi_{y,x} \\ 0 \\ 0 \end{Bmatrix} \tag{8}$$

where in the above equations $()_{,x}$ and $()_{,y}$ denote the derivatives with respect to the x and y directions, respectively.

For linear thermoelastic materials, stress field may be written as a linear function of strain field and temperature change as

$$\begin{Bmatrix} \sigma_{xx} \\ \sigma_{yy} \\ \tau_{yz} \\ \tau_{xz} \\ \tau_{xy} \end{Bmatrix} = \begin{bmatrix} Q_{11} & Q_{12} & 0 & 0 & 0 \\ Q_{12} & Q_{22} & 0 & 0 & 0 \\ 0 & 0 & Q_{44} & 0 & 0 \\ 0 & 0 & 0 & Q_{55} & 0 \\ 0 & 0 & 0 & 0 & Q_{66} \end{bmatrix} \times \begin{Bmatrix} \varepsilon_{xx} - \alpha_{11}\Delta T \\ \varepsilon_{yy} - \alpha_{22}\Delta T \\ \gamma_{yz} \\ \gamma_{xz} \\ \gamma_{xy} \end{Bmatrix} \tag{9}$$

where, T and T_0 are, respectively, the elevated temperature and reference temperature, respectively.

Besides, Q_{ij}'s $(i,j=1,2,4,5,6)$ are the reduced material stiffness coefficients compatible with the plane-stress conditions and are obtained as follow [49]

$$Q_{11}=\frac{E_{11}}{1-v_{12}v_{21}},\quad Q_{22}=\frac{E_{22}}{1-v_{12}v_{21}},$$
$$Q_{12}=\frac{v_{21}E_{11}}{1-v_{12}v_{21}},\quad Q_{44}=G_{23},\quad Q_{55}=G_{13},$$
$$Q_{66}=G_{12} \tag{10}$$

and loading type. However, approximate values of $\kappa=1$, $\kappa=5/6$ or $\kappa=\pi^2/12$ are used extensively. In this research, the shear correction factor is set equal to $\kappa=5/6$.

Substitution of Eq. (9) into Eq. (11) with the simultaneous aid of Eqs. (5)–(8), and (10) generates the stress resultants in terms of the mid-surface characteristics of the plate as

$$\begin{Bmatrix} N_{xx}\\ N_{yy}\\ N_{xy}\\ M_{xx}\\ M_{yy}\\ M_{xy}\\ Q_{yz}\\ Q_{xz}\end{Bmatrix}=\begin{bmatrix} A_{11} & A_{12} & 0 & B_{11} & B_{12} & 0 & 0 & 0\\ A_{12} & A_{22} & 0 & B_{12} & B_{22} & 0 & 0 & 0\\ 0 & 0 & A_{66} & 0 & 0 & B_{66} & 0 & 0\\ B_{11} & B_{12} & 0 & D_{11} & D_{12} & 0 & 0 & 0\\ B_{12} & B_{22} & 0 & D_{12} & D_{22} & 0 & 0 & 0\\ 0 & 0 & B_{66} & 0 & 0 & D_{66} & 0 & 0\\ 0 & 0 & 0 & 0 & 0 & 0 & \kappa A_{44} & 0\\ 0 & 0 & 0 & 0 & 0 & 0 & 0 & \kappa A_{55}\end{bmatrix}\begin{Bmatrix} \varepsilon_{xx0}\\ \varepsilon_{yy0}\\ \gamma_{xy0}\\ \kappa_{xx}\\ \kappa_{yy}\\ \kappa_{xy}\\ \gamma_{yz0}\\ \gamma_{xz0}\end{Bmatrix}-\begin{Bmatrix} N^T_{xx}\\ N^T_{yy}\\ 0\\ M^T_{xx}\\ M^T_{yy}\\ 0\\ 0\\ 0\end{Bmatrix} \tag{12}$$

Stress resultants of the FSDT may be obtained upon integration of stress field through the thickness. Stress resultant components in this case become [48]

$$\begin{Bmatrix} N_{xx}\\ N_{yy}\\ N_{xy}\\ M_{xx}\\ M_{yy}\\ M_{xy}\\ Q_{xz}\\ Q_{yz}\end{Bmatrix}=\int_{-0.5h}^{+0.5h}\begin{Bmatrix} \sigma_{xx}\\ \sigma_{yy}\\ \tau_{xy}\\ z\sigma_{xx}\\ z\sigma_{yy}\\ z\tau_{xy}\\ \kappa\tau_{xz}\\ \kappa\tau_{yz}\end{Bmatrix}dz \tag{11}$$

In the above equation, κ is the shear correction factor of FSDT. As known, adoption of a shear correction factor results in more accurate buckling loads and somehow compensate the errors due to the assumption of uniform transverse strains. Evaluation of accurate shear correction factor for FG-CNTRC plates is not straightforward since this factor depends on the boundary conditions, material properties, geometry

In the above equation, the stiffness components A_{ij}, B_{ij}, and D_{ij} indicate the stretching, bending-stretching, and bending stiffnesses, respectively, which are calculated by

$$\left(A_{ij},B_{ij},D_{ij}\right)=\int_{-0.5h}^{+0.5h}\left(Q_{ij},zQ_{ij},z^2Q_{ij}\right)dz \tag{13}$$

Also, $N^T_{ii}, M^T_{ii}, i=,x,y$ are the thermally induced force and moment resultants which are obtained upon calculation of stress resultants as

$$\begin{bmatrix} N^T_{xx} & M^T_{xx}\\ N^T_{yy} & M^T_{yy}\end{bmatrix}=\int_{-0.5h}^{+0.5h}\begin{bmatrix} Q_{11} & Q_{12}\\ Q_{12} & Q_{22}\end{bmatrix}\begin{bmatrix} \alpha_{11}\\ \alpha_{22}\end{bmatrix}(T-T_0)dz \tag{14}$$

It is of worth-noting that, under uniform temperature rise and for FG-X, FG-O and UD types of CNT distribution, no thermal bending moments are produced. Besides, due to the symmetric distribution of CNTs across the thickness in these three cases, the stretching-bending coupling stiffness components, i.e. B_{ij}'s are all equal to zero.

Stability equations of the plate may be obtained with the aid of static version of the Hamilton principle [48]. At the onset of buckling, one may write

$$\delta(U+V)=0 \tag{15}$$

where δU is the virtual strain energy of the thermoelastic plate which may be calculated as

$$\delta U=\int_{-0.5a}^{+0.5a}\int_{-0.5b}^{+0.5b}\int_{-0.5h}^{+0.5h}\left(\sigma_{xx}\delta\varepsilon_{xx}+\sigma_{yy}\delta\varepsilon_{yy}+\tau_{xy}\delta\gamma_{xy}+\kappa\tau_{xz}\delta\gamma_{xz}+\kappa\tau_{yz}\delta\gamma_{yz}\right)dzdydx \tag{16}$$

and δV is the virtual potential energy of the prebuckling loads due to the constant uniform heating. It is of worth-noting that, even under uniform heating, bifurcation phenomenon may not occur. Considering the distributed patterns of CNTs across the plate thickness, in this study, three symmetric patterns and one nonsymmetric pattern are taken into consideration. As mentioned earlier in FG-V type of CNT dispersion and even in uniform heating, thermal moments are generated. Obviously, the induced thermal moments enforce the plate to deflect unless the thermally induced moments are surpassed by the supports. As known, clamped and sliding supported edges are capable of applying the additional bending moment at the support when is necessary, however, simply supported and free edges are unable to reveal such feature. Therefore, thermal buckling occurs for arbitrary type of FG-CNTRC plate with combinations of clamped and sliding supported edges. However, for plates with at least one edge simply supported or free, distribution of CNTs across the thickness should be symmetric.

Considering that the above conditions are met for the occurrence of thermal bifurcation buckling, prebuckling forces may be obtained according to the in-plane boundary conditions. For the case when in-plane displacement components are equal to zero at the edges (all edges are restrained again thermal expansion), prebuckling forces are equal to thermally induced loads. Therefore, the potential energy of the prebuckling forces at the onset of buckling is equal to

$$\delta V=-\int_{-0.5a}^{+0.5a}\int_{-0.5b}^{+0.5b}\left(N_{xx}^{T}w_{0,x}\delta w_{0,x}+N_{yy}^{T}w_{0,y}\delta w_{0,y}\right)dydx \tag{17}$$

However, when two parallel edges of the plate are not restrained to move in normal to edge direction, in that direction, only thermal expansion is generated and thermal forces are not induced. In this case, prebuckling thermal forces should be obtained using the same process developed by Jones [50]. In a plate with free boundary conditions along $y=\pm b/2$, while the two other edges are restrained against thermal expansion, the prebuckling forces are obtained by Jones [50]. The work done by such thermally induced forces at the onset of buckling may be written as

$$\delta V=-\int_{-0.5a}^{+0.5a}\int_{-0.5b}^{+0.5b}\left(\frac{A_{11}}{A_{22}}N_{yy}^{T}-N_{xx}^{T}\right)w_{0,x}\delta w_{0,x}dydx \tag{18}$$

3 Solution procedure

While the stability equations and the associated boundary conditions may be obtained through the application of Green theorem to the expression (15), energy based methods also may be used to solve the stability equation (15). In the present research, Ritz method with Chebyshev basis polynomials is used to derive the stability equations in a matrix representation. Accordingly, each of the essential variables may be expanded via Chebyshev polynomials and auxiliary functions such that

$$\begin{aligned}
u_0(x,y)&=R^{u}(x,y)\sum_{i=1}^{N_x}\sum_{j=1}^{N_y}U_{ij}P_i(x)P_j(y)\\
v_0(x,y)&=R^{v}(x,y)\sum_{i=1}^{N_x}\sum_{j=1}^{N_y}V_{ij}P_i(x)P_j(y)\\
w_0(x,y)&=R^{w}(x,y)\sum_{i=1}^{N_x}\sum_{j=1}^{N_y}W_{ij}P_i(x)P_j(y)\\
\varphi_x(x,y)&=R^{x}(x,y)\sum_{i=1}^{N_x}\sum_{j=1}^{N_y}X_{ij}P_i(x)P_j(y)\\
\varphi_y(x,y)&=R^{y}(x,y)\sum_{i=1}^{N_x}\sum_{j=1}^{N_y}Y_{ij}P_i(x)P_j(y)
\end{aligned} \tag{19}$$

where in the above equation $P_i(x)$ and $P_j(y)$ are the i-th and $j-$th Chebyshev polynomials of the first kind which are defined by

$$P_i(x) = \cos((i-1)\arccos(2x/a))$$
$$P_j(y) = \cos((j-1)\arccos(2y/b)) \quad (20)$$

Besides, functions $R^{\alpha}(x,y), \alpha = u,v,w,x,y$ are the boundary functions corresponding to the essential boundary conditions. It is known that in Ritz family methods, adoption of a shape function depends only on the essential boundary condition. Four types of boundary conditions are used in this study. clamped (C), simply supported (S), free (F) and sliding supported (X). For a clamped edge all of the in-plane and out-of-plane essential variables are restrained. For a simply supported edge normal and tangential displacements, lateral displacement and tangential slope are restrained and for a sliding supported edge only normal slope is restrained. At a free edge none of the boundary conditions are essential. Therefore, the essential variables associated to each of these cases may be written as

For a clamped edge:
$x = \pm a/2: u_0 = v_0 = w_0 = \varphi_x = \varphi_y = 0$
$y = \pm b/2: u_0 = v_0 = w_0 = \varphi_x = \varphi_y = 0$
For a simply supported edge:
$x = \pm a/2: u_0 = v_0 = w_0 = \varphi_y = 0$
$y = \pm b/2: u_0 = v_0 = w_0 = \varphi_x = 0$
For a sliding supported edge:
$x = \pm a/2: u_0 = v_0 = \varphi_x = 0$
$y = \pm b/2: u_0 = v_0 = \varphi_y = 0$
For a free edge:
$x = \pm a/2: -$
$y = \pm b/2: -$ (21)

The shape functions of the Ritz method should be chosen according to the above essential variables. All of the Chebyshev functions are nonzero at both ends of the interval. Therefore, auxiliary functions $R^{\alpha}, \alpha = u,v,w,x,y$ should satisfy the essential boundary conditions on each edge of the plate. Each of the functions $R^{\alpha}, \alpha = u,v,w,x,y$ may be written as

$$R^{\alpha}(x,y) = \left(1+\frac{2x}{a}\right)^{p}\left(1-\frac{2x}{a}\right)^{q}\left(1+\frac{2y}{b}\right)^{r}\left(1-\frac{2y}{b}\right)^{s} \quad (22)$$

Each of the variables p, q, r and s depends on the essential boundary conditions and are equal to zero or one. For instance in a plate with clamped boundaries on $x = -0.5a$ and $x = +0.5a$, simply supported at $y = -0.5b$ and sliding supported at $y = +0.5b$, auxiliary functions are as

$$R^{u}(x,y) = \left(1+\frac{2x}{a}\right)\left(1-\frac{2x}{a}\right)\left(1+\frac{2y}{b}\right)\left(1-\frac{2y}{b}\right)$$
$$R^{v}(x,y) = \left(1+\frac{2x}{a}\right)\left(1-\frac{2x}{a}\right)\left(1+\frac{2y}{b}\right)\left(1-\frac{2y}{b}\right)$$
$$R^{w}(x,y) = \left(1+\frac{2x}{a}\right)\left(1-\frac{2x}{a}\right)\left(1+\frac{2y}{b}\right)$$
$$R^{x}(x,y) = \left(1+\frac{2x}{a}\right)\left(1-\frac{2x}{a}\right)\left(1+\frac{2y}{b}\right)$$
$$R^{y}(x,y) = \left(1+\frac{2x}{a}\right)\left(1-\frac{2x}{a}\right)\left(1-\frac{2y}{b}\right) \quad (23)$$

Finally substitution of Eq. (19) into the Eqs. (15) results in an eigenvalue problem as

$$(\mathbf{K^e} - \mathbf{K^g})\mathbf{X} = \mathbf{0} \quad (24)$$

where $\mathbf{K^e}$ is the elastic stiffness matrix which is originated from Eq. (16) and $\mathbf{K^g}$ is originated from the geometrical stiffness matrix from Eqs. (17) or (18). Each of these matrices has $5 \times N_x \times N_y$ rows and columns. The above system should be treated as a standard eigenvalue problem to obtain the critical buckling temperature. It should be mentioned that, since the temperature dependency of the constituents is taken into consideration, a successive procedure should be carried out to obtain the critical buckling temperature. To initiate the process, at first, thermo-mechanical properties of the CNTs and matrix are evaluated at reference temperature. Thermomechanical properties are then computed at the obtained temperature and the eigenvalue problem is repeated again to extract a new critical buckling temperature. This procedure continues until a converged critical buckling temperature is achieved.

4 Numerical results and discussion

Present study aims to analyse the thermal buckling behaviour of FG-CNTRC moderately thick rectangular plates with temperature dependent material properties. In this section, at first, convergence and comparison studies are conducted. Afterwards,

parametric studies are performed to examine the influences of involved parameters. In the rest of this manuscript the following convention is established for boundary conditions. For instance, in an SCSX plate, the first letter is associated to $x = -0.5a$, the second letter is the boundary condition at $y = -0.5b$, the third letter denotes the boundary conditions at $x = +0.5a$ and finally the last letter is associated with the boundary at $y = +0.5b$. Unless otherwise stated, Poly (methyl methacrylate), referred to as PMMA, is selected for the matrix with material properties $E^m = (3.52 - 0.0034T)$ GPa, $\nu^m = 0.34$ and $\alpha^m = 45(1+0.0005\Delta T)10^{-6}$/K. In calculation of elasticity modulus of matrix $T = T_0 + \Delta T$ where $T_0 = 300$ K is the reference temperature and T is measured in Kelvin. (10,10) armchair SWCNT is chosen as the reinforcement. Elasticity modulus, shear modulus, Poisson's ratio and thermal expansion coefficient of SWCNT are highly dependent to temperature. Shen and Xiang [51] reported these properties at four certain temperature levels, i.e. $T = 300, 400, 500$ and 700 K. The magnitudes of $E_{11}, E_{22}, G_{12}, \alpha_{11}, \alpha_{22}$ and ν_{12} for CNTs at these four specific temperatures are given in Table 2.

Since this study aims to analyse the critical buckling temperature of FG-CNTRC plates under temperature dependent assumptions, it is necessary to obtain the thermomechanical properties of CNTs as a continuous function of temperature. For this purpose, for each of the thermomechanical properties of the CNT, a third order interpolation is done to obtain the properties of CNT as a function of temperature. As a result of interpolation, each of the properties may be written as

$$
\begin{aligned}
E_{11}^{CN}(T)(\text{TPa}) &= 6.3998 - 4.338417 \times 10^{-3}T + 7.43 \\
&\quad \times 10^{-6}T^2 - 4.458333 \times 10^{-9}T^3 \\
E_{22}^{CN}(T)(\text{TPa}) &= 8.02155 - 5.420375 \times 10^{-3}T \\
&\quad + 9.275 \times 10^{-6}T^2 - 5.5625 \times 10^{-9}T^3 \\
G_{12}^{CN}(T)(\text{TPa}) &= 1.40755 + 3.476208 \times 10^{-3}T \\
&\quad - 6.965 \times 10^{-6}T^2 + 4.479167 \times 10^{-9}T^3 \\
\alpha_{11}^{CN}(T)(10^{-6}/\text{K}) &= -1.12515 + 0.02291688T \\
&\quad - 2.887 \times 10^{-5}T^2 + 1.13625 \times 10^{-8}T^3 \\
\alpha_{22}^{CN}(T)(10^{-6}/\text{K}) &= 5.43715 - 0.9.84625 \times 10^{-4}T \\
&\quad + 2.9 \times 10^{-7}T^2 + 1.25 \times 10^{-11}T^3 \\
\nu_{12}^{CN} &= 0.175
\end{aligned}
\tag{25}
$$

Han and Elliott [52] performed a molecular dynamics simulation to obtain the mechanics properties of nanocomposites reinforced with SWCNT. However in their analysis, the effective thickness of CNT is assumed to be at least 0.34 nm. The thickness of CNT as reported should be at least 0.142 nm [53]. Therefore molecular dynamics simulation of Han and Elliott [52] is re-examined [43]. The so-called efficiency parameters, as stated earlier, are chosen to match the data obtained by the modified rule of mixture of the present study and the molecular dynamics simulation results [43]. For three different volume fractions of CNTs, these parameters are as: $\eta_1 = 0.137$ and $\eta_2 = 1.022$ for $V_{CN}^* = 0.12$. $\eta_1 = 0.142$ and $\eta_2 = 1.626$ for $V_{CN}^* = 0.17$. $\eta_1 = 0.141$ and $\eta_2 = 1.585$ for $V_{CN}^* = 0.28$. For each case, the efficiency parameter η_3 is equal to $0.7\eta_2$. The shear modulus G_{13} is taken equal to G_{12} whereas G_{23} is taken equal to $1.2G_{12}$ [43].

4.1 Convergence and comparison studies

In this section, convergence and comparison studies are provided. At first a convergence study is given to obtain the required number of shape functions in series expansion of the Ritz method. Convergence study is provided in Table 3. For this purpose, critical buckling temperature parameter of isotropic homogeneous plates with all edges simply supported are evaluated

Table 2 Thermo-mechanical properties of (10,10) armchair SWCNT at specific temperatures [51] (tube length = 9.26 nm, tube mean radius = 0.68 nm, tube thickness = 0.067 nm)

T (K)	E_{11}^{CN}(TPa)	E_{22}^{CN}(TPa)	G_{12}^{CN}(TPa)	ν_{12}^{CN}	$\alpha_{11}^{CN}(10^{-6}/\text{K})$	$\alpha_{22}^{CN}(10^{-6}/\text{K})$
300	5.6466	7.0800	1.9445	0.175	3.4584	5.1682
400	5.5679	6.9814	1.9703	0.175	4.1496	5.0905
500	5.5308	6.9348	1.9643	0.175	4.5361	5.0189
700	5.4744	6.8641	1.9644	0.175	4.6677	4.8943

Table 3 Convergence study for critical buckling temperature parameter $1000\Delta T_{cr}\alpha$ of isotropic homogeneous SSSS square plates with $v = 0.21$ and various side to thickness ratios

(N_x, N_y)	$a/h = 100$	$a/h = 20$	$a/h = 10$	$a/h = 5$
(3,3)	0.1409	3.4700	13.2507	44.9211
(4,4)	0.1265	3.1209	11.9835	41.3139
(5,5)	0.1265	3.1209	11.9835	41.3138
(6,6)	0.1265	3.1200	11.9801	41.3038
(7,7)	0.1265	3.1200	11.9799	41.3033
(8,8)	0.1265	3.1200	11.9799	41.3033
(9,9)	0.1265	3.1199	11.9795	41.3016
(10,10)	0.1265	3.1199	11.9795	41.3016
Shen [54]	0.1265	3.1194	11.978	41.297

for various number of the assumed shape functions. Results are compared with those obtained by Shen [54] based on an exact analytical solution. It is seen than Ritz method always serves an upper bound for the critical buckling temperatures of the plate. Furthermore, After adoption of 10 shape functions in both x and y directions highly accurate numerical results are achieved. Consequently, in the rest of this work, number of shape functions in Ritz approximation is set equal to $N_x = N_y = 10$.

A comparison is presented in Table 4 on critical buckling temperature parameter of cross-ply symmetric laminated plates. For the sake of comparison, characteristics of the plate are set equal to those from the references. A square plate made of an orthotropic material with material properties $E_{11} = 15E_{22}$, $G_{12} = G_{13} = 0.5E_{22}$, $G_{23} = 0.3356E_{22}$, $\nu_{12} = 0.3$ and $\alpha_{11} = 0.015\alpha_{22}$ is considered. Critical buckling temperature difference parameter in this comparison is defined as $\Delta T\alpha_{22}$. Results of this study are presented for two layering schemes, namely [0] and [0/90/0]. In each case two width to thickness ratios are assumed. Results of the present research are compared with the results of Matsunaga [55] based on a global higher-order theory, three-dimensional elasticity-based results of Noor and Burton [56], and results of Singh et al. [57] based on meshless finite element method using third order theory. It is seen that, numerical results of this study match well with the aforementioned works which accepts the accuracy and effectiveness of the proposed solution and formulation in the present study.

One of the available researches on thermal buckling of CNTRC rectangular plates belongs to Shen and Zhang [23]. In the study of Shen and Zhang exact solution is presented to obtain the critical buckling temperature of FG-CNTRC plates with all edges simply-supported and symmetric pattern of CNT dispersion across the plate thickness. Unlike the present case, Shen and Zhang [23] used the classical rule of mixtures to obtain the longitudinal thermal expansion coefficient of the CNTRC. Therefore only in this example and for the sake of comparison, longitudinal thermal expansion coefficient is evaluated as

$$\alpha_{11} = V_{CN}\alpha_{11}^{CN} + V_m\alpha^m \tag{26}$$

Critical buckling temperature of FG-CNTRC plates with two different side to thickness ratios and three different length to side ratios are evaluated and compared with those of Shen and Zhang [23]. Comparison is carried out in Table 5. It is seen that results of our study match well with those of Shen and Zhang [23].

4.2 Parametric studies

After validating the numerical results of this study with the available data in the open literature, parametric studies are conducted in this section. Numerical results are provided in Tables 6, 7, 8 and 9 and Figs. 1 and 2. In all of this section, critical buckling temperature is obtained under the assumption of temperature dependent material properties.

Table 6 presents the critical buckling temperature of FG-CNTRC plates. In this table, various combinations of simply supported and clamped conditions are

Table 4 Comparison of critical buckling temperature difference parameter, $\Delta T_{cr}\alpha_{22}$ for square SSSS cross-ply laminates

Lay-up	b/h	Present	Matsunaga [55]	Noor and Burton [56]	Singh et al. [57]
[0]	100	0.7469×10^{-3}	0.7463×10^{-3}	0.7463×10^{-3}	0.7463×10^{-3}
	20	0.1739×10^{-1}	0.1739×10^{-1}	0.1771×10^{-1}	0.1752×10^{-1}
[0/90/0]	100	0.9921×10^{-3}	0.9910×10^{-3}	0.9961×10^{-3}	0.9917×10^{-3}
	20	0.2346×10^{-1}	0.2291×10^{-1}	0.2308×10^{-1}	0.2308×10^{-1}

Table 5 Critical buckling temperature, $T_{cr}(K)$ of SSSS FG-CNTRC rectangular plates with $V^*_{CN} = 0.17$ and temperature dependent material properties

a/*b*, *b*/*h*	Type	Present	Shen and Zhang [23]
1.0,20	UD	343.00	343.00
	FG-X	359.43	359.52
1.5,20	UD	325.08	325.08
	FG-X	335.14	335.54
2.0,20	UD	319.03	319.01
	FG-X	325.68	326.16
1.0,10	UD	399.03	399.44
	FG-X	419.13	419.09
1.5,10	UD	374.66	374.59
	FG-X	394.42	394.66
2.0,10	UD	363.86	363.67
	FG-X	380.94	377.46

Various side to thickness and aspect ratios are considered

considered for the edges of the plate. As stated earlier, thermal bifurcation buckling in plates with at least one edge simply supported takes place when distribution of CNTs across the thickness is symmetric with respect to the mid-plane. Therefore, only FG-X, FG-O and UD CNTRC plates are considered. Three different patterns of the CNT dispersion and three different magnitudes of volume fraction of CNTs are considered. A square plate with length to thickness ratio $a/h = 30$ is considered. From the numerical results of this table it is concluded that, for all cases, FG-X plates have higher buckling temperature than UD case and the latter dispersion profile results in higher buckling temperature in comparison to plates with FG-O type of CNT dispersion. For all of the studied cases in this table, increasing the volume fraction of CNT results in higher critical buckling temperature. However the influence of volume fraction of CNTs on critical

Table 6 Thermal buckling temperature $T_{cr}(K)$ for square FG-CNTRC plates with $a/h = 30$, various volume fraction of CNTs, different graded pattern and combinations of S and C edges

Boundary conditions	Type	$V^*_{CN} = 0.12$	$V^*_{CN} = 0.17$	$V^*_{CN} = 0.28$
SSSS	UD	420.3703	422.6275	434.4771
	FG-X	449.0291	453.5322	474.6826
	FG-O	379.9912	379.7433	385.6686
SCSC	UD	437.8200	440.0585	447.4740
	FG-X	476.9579	482.0888	493.8651
	FG-O	389.8706	390.8179	393.8727
SCSS	UD	426.5649	428.5238	438.9547
	FG-X	456.8312	462.4126	481.9622
	FG-O	381.8417	381.9920	387.2202
CCCC	UD	561.5707	571.5140	577.8439
	FG-X	597.0642	614.4112	625.7757
	FG-O	501.0371	504.8352	513.7900
CSCS	UD	538.6131	547.5073	561.6472
	FG-X	568.3926	584.3437	609.6522
	FG-O	483.0916	485.0283	498.3931
CCCS	UD	543.5920	552.3654	563.5335
	FG-X	575.2267	591.4898	610.3639
	FG-O	485.9552	488.5219	500.7041
CCSS	UD	481.6283	486.2792	498.6593
	FG-X	516.0845	525.9173	545.7405
	FG-O	431.4170	432.6502	440.5358
CCSC	UD	498.7899	505.2330	515.1643
	FG-X	533.4550	545.5234	564.5335
	FG-O	442.5950	444.1633	449.4430
CSSS	UD	476.9768	480.6302	493.3922
	FG-X	514.7671	522.9329	540.0177
	FG-O	425.0026	425.9865	434.9565

Table 7 Thermal buckling temperature $T_{cr}(K)$ for square FG-CNTRC plates with $a/h = 30$, various volume fraction of CNTs, different graded pattern and combinations of X and C edges

Boundary conditions	Type	$V^*_{CN} = 0.12$	$V^*_{CN} = 0.17$	$V^*_{CN} = 0.28$
CCCC	UD	561.5707	571.5140	577.8439
	FG-X	597.0642	614.4112	625.7757
	FG-O	501.0371	504.8352	513.7900
	FG-V	529.5172	537.3850	550.7551
CCCX	UD	541.5753	550.1713	562.0526
	FG-X	574.0102	589.6564	609.1062
	FG-O	487.0667	489.9096	501.5818
	FG-V	516.4236	523.7059	540.5338
CXCX	UD	545.7897	555.3589	566.3932
	FG-X	575.1468	591.9157	612.1900
	FG-O	482.9084	484.8447	498.1785
	FG-V	517.5165	523.0890	537.1724
CCXC	UD	410.4058	411.9697	425.6823
	FG-X	437.1615	441.0613	464.6675
	FG-O	378.9807	379.7285	384.9231
	FG-V	392.5021	394.5453	405.6597
CCXX	UD	391.5104	392.9325	407.4350
	FG-X	410.6407	414.2345	439.8130
	FG-O	367.6227	367.6345	374.4760
	FG-V	381.2169	383.0962	395.8041
CXXX	UD	390.2247	392.5502	406.1927
	FG-X	405.5669	410.2949	436.4458
	FG-O	358.2722	357.1367	366.6267
	FG-V	375.6559	374.8235	388.1690
XCXC	UD	364.7833	368.1326	376.8900
	FG-X	369.1066	375.4019	396.1049
	FG-O	361.4049	362.9827	366.1939
	FG-V	365.4714	369.4561	380.7864
XCXX	UD	316.7557	317.6388	319.9532
	FG-X	317.9081	319.5818	325.1344
	FG-O	315.8585	316.2683	317.0876
	FG-V	316.9551	318.0286	321.1583

buckling temperature is not comparable to the influence of CNT dispersion pattern. It is observed that, maximum buckling temperature belongs to a plate with all edges clamped and the minimum one belongs to the one with all edges simply supported. This is expected since clamping results in higher local flexural rigidity in comparison to simply supported edge. Considering the fact that FG-CNTRC plates are orthotropic, as seen, buckling temperature of CCCS and CCSC plates are not equal. Considering various combinations of clamped and simply supported boundary conditions in square plates, numerical results reveal that critical buckling temperature may be sorted from high to low in plates with the following boundary conditions: CCCC, CCCS, CSCS, CCSC, CCSS, CSSS, SCSC, SCSS, SSSS.

Table 7 presents the critical buckling temperature of FG-CNTRC plates with combinations of clamped and sliding supported edge. Both clamped and sliding support boundary conditions, are capable of applying the additional bending moment in the prebuckling state and therefore plate remains flat even when the

Table 8 Critical buckling temperatures $T_{cr}(K)$ for SSSS FG-CNTRC plates with FG-X type of CNT dispersion, various aspect and side to thickness ratios

a/b	b/h	$V^*_{CN} = 0.12$	$V^*_{CN} = 0.17$	$V^*_{CN} = 0.28$
0.8	100	326.4442	326.8382	332.7388
	50	395.8360	396.5316	411.9645
	30	511.8921	518.8456	533.8224
	20	630.6262	650.2838	643.5145
1.0	100	316.6240	316.7554	320.8529
	50	361.9401	362.8735	375.7231
	30	449.0291	453.5322	474.6826
	20	565.0145	579.0660	593.6007
1.2	100	311.8853	312.2107	315.2405
	50	345.3733	346.7878	357.1273
	30	414.3599	418.8973	439.4821
	20	518.6412	530.4655	541.5596
1.5	100	308.1456	308.0527	309.9251
	50	331.2706	331.0456	337.5244
	30	379.7663	379.9137	393.1864
	20	455.9459	458.7011	475.5308
2.0	100	304.2378	304.2632	305.3594
	50	316.6240	316.7554	320.8529
	20	344.2250	344.7655	354.5800
	10	392.2411	394.0970	411.0742

distribution of material properties is not symmetric with respect to the mid-plane. Consequently, plates with combinations of C or X edges, and subjected to arbitrary type of CNT dispersion reveal the thermal bifurcation buckling. In this table, four cases of CNT dispersion and three types of volume fraction of CNTs are considered. Square plates with width to thickness ratio $a/h = 30$ are under investigation. It is seen that, critical buckling temperature of FG-V plate is also lower than those with FG-X type of CNT dispersion. Therefore from this table and Table 6 it is concluded that, FG-X type of CNT dispersion is the most influential type in thermal stability. It is observed that critical buckling temperature in FG-CNTRC plates decreases permanently when profile of the CNT through the thickness changes in order from FG-X to UD, then FG-V and finally FG-O. The key issue in higher buckling temperature of FG-X plates in comparison to the three other cases is the fact that, bending stiffnesses of the plate are much more in FG-X case since in the latter case the surfaces that are far from the mid-plane are much more enriched with CNT.

Table 9 Critical buckling temperatures $T_{cr}(K)$ for FG-CNTRC plates with two parallel edges free, various types of CNT dispersion, $V^*_{CN} = 0.12$, $b/h = 50$ and various aspect ratios

a/b	b/h	CFCF	SFSF	CFSF	CFXF
0.8	UD	588.9004	409.4219	486.2655	409.4667
	FG-X	648.6430	449.2390	541.5037	449.2726
	FG-O	488.5555	362.2013	412.5338	362.2621
1.0	UD	520.4770	375.5222	434.2592	375.5639
	FG-X	581.5349	404.9044	479.8350	404.9379
	FG-O	435.3279	341.8365	378.0741	341.8900
1.2	UD	470.7697	355.0346	400.6470	355.0723
	FG-X	525.2763	377.4119	437.4189	377.4431
	FG-O	401.2215	329.9460	357.0731	329.9919
1.5	UD	421.3874	336.8435	369.3452	336.8741
	FG-X	464.5090	352.5080	396.4552	352.5343
	FG-O	369.6185	318.8456	338.3172	319.7243
2.0	UD	375.5660	321.5654	341.7839	321.5859
	FG-X	404.9405	331.1463	359.2432	331.1646
	FG-O	341.8910	311.3281	332.4832	311.3500

Tables 8 present the critical buckling temperatures of SSSS FG-CNTRC plates with various aspect ratios and also various side to thickness ratios. Three different magnitudes are considered for the volume fraction of CNTs whereas dispersion of CNTs is of FG-X type. Numerical results of this table reveal that, similar to square plate, increasing the volume fraction of CNTs enhances the buckling temperature of the plate. Besides, when width and thickness of the plate are constant, increasing the length of the plate results in lower critical buckling temperature.

An example of thermal buckled shapes of FG-CNTRC plates with FG-X type of CNT dispersion is presented in Fig. 1. Square plates with various boundary conditions comprising of C and X type of edges, side to thickness ratio $a/h = 30$ and volume fraction $V^*_{CN} = 0.28$ are considered. It is seen that essential boundary conditions are satisfied at the supports since at the sliding supported edge lateral displacement is not restrained. Unlike the case of fully clamped square isotropic plate which thermally buckles in a double symmetric shape, FG-CNTRC CCCC plate buckles in a shape which is symmetric along the x direction and antisymmetric along the y direction.

Table 9 is devoted to the case of plates where two parallel edges are free and the two others are restrained

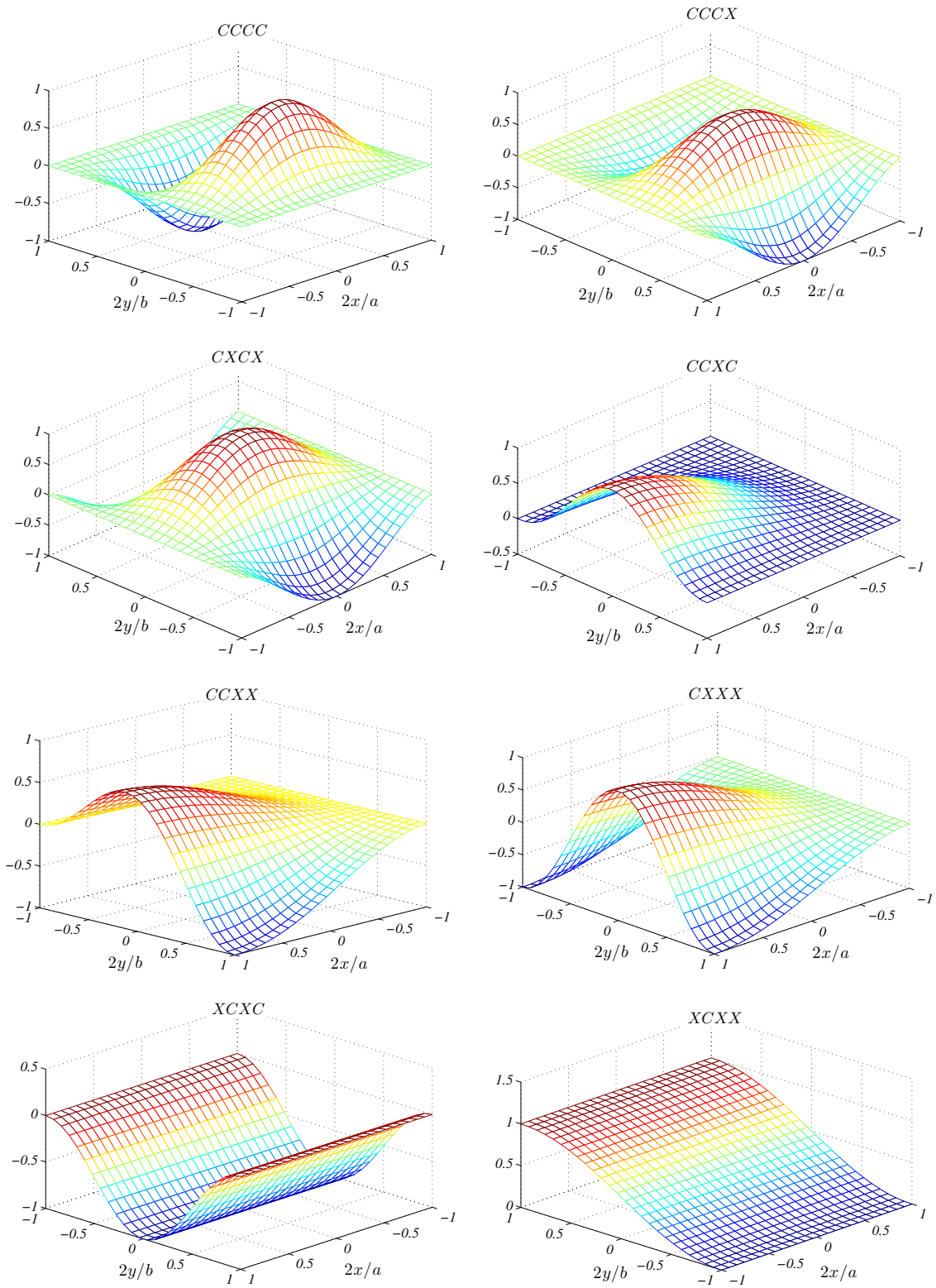

Fig. 1 Lateral displacement mode shape of FG-CNTRC square plates with FG-X type of CNT dispersion, $a/h = 30$, volume fraction $V^*_{CN} = 0.28$ and various boundary conditions

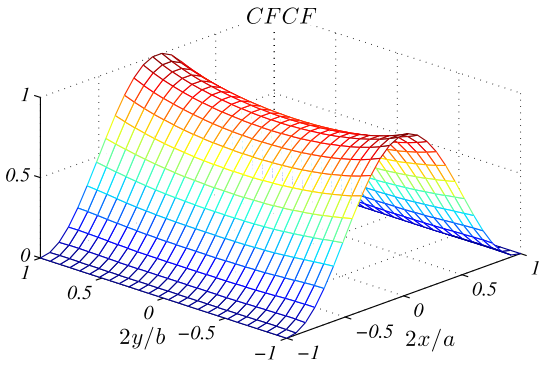
CFCF
1
0.5
0
1
0.5
0
2y/b −0.5
−1 −1
−0.5 2x/a
0
0.5
1

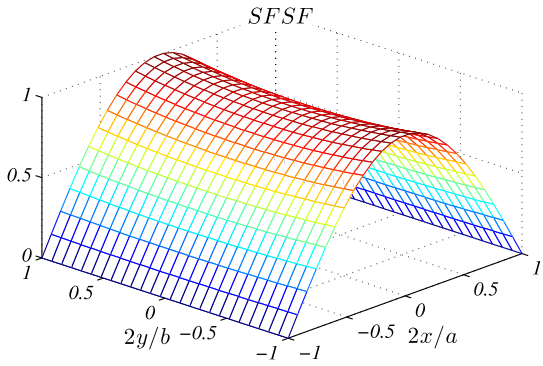
SFSF
1
0.5
0
1
0.5
0
2y/b −0.5
−1 −1
−0.5 2x/a
0
0.5
1

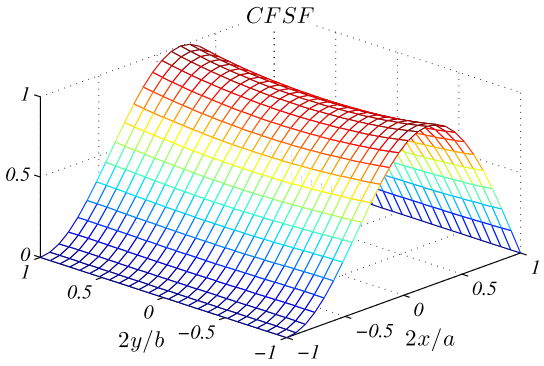
CFSF
1
0.5
0
1
0.5
0
2y/b −0.5
−1 −1
−0.5 2x/a
0
0.5
1

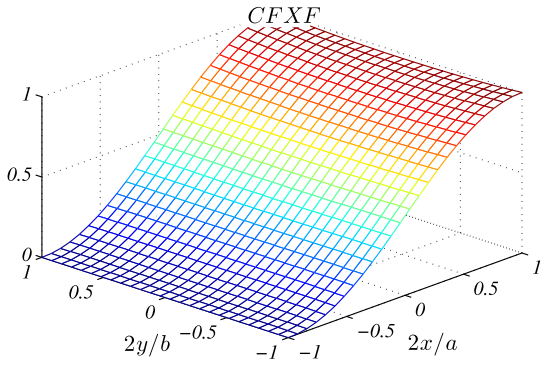
CFXF
1
0.5
0
1
0.5
0
2y/b −0.5
−1 −1
−0.5 2x/a
0
0.5
1

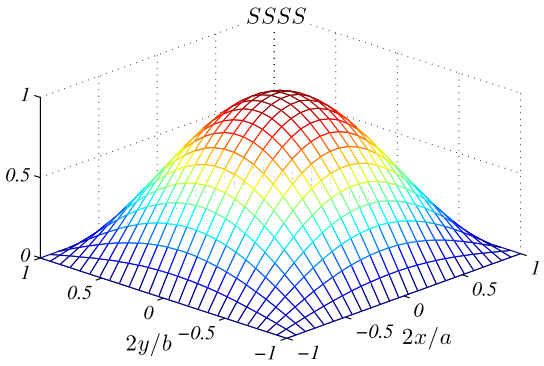
SSSS
1
0.5
0
1
0.5
0
2y/b −0.5
−1 −1
−0.5 2x/a
0
0.5
1

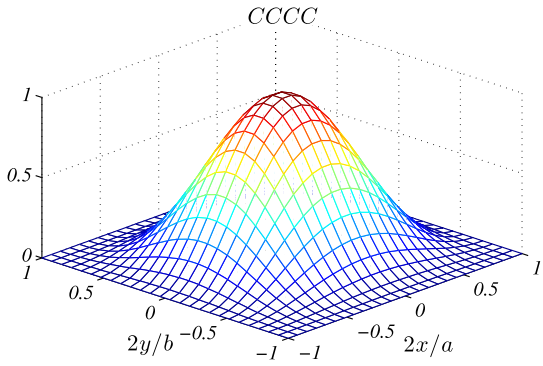
CCCC
1
0.5
0
1
0.5
0
2y/b −0.5
−1 −1
−0.5 2x/a
0
0.5
1

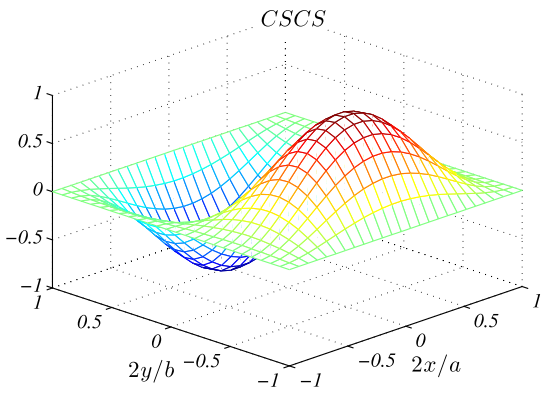
CSCS
1
0.5
0
−0.5
−1
1
0.5
0
2y/b −0.5
−1 −1
−0.5 2x/a
0
0.5
1

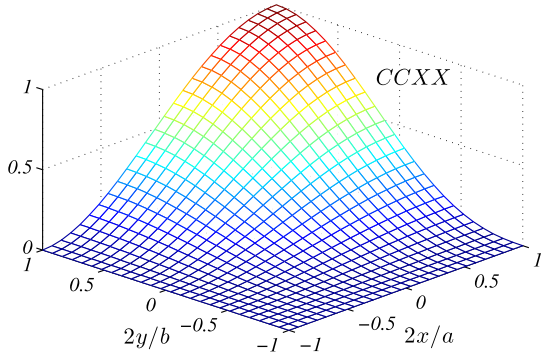
CCXX
1
0.5
0
1
0.5
0
2y/b −0.5
−1 −1
−0.5 2x/a
0
0.5
1

◀**Fig. 2** Lateral displacement mode shape of FG-CNTRC rectangular plates with $a/b = 2$, FG-X type of CNT dispersion, $a/h = 50$, volume fraction $V^*_{CN} = 0.12$ and various boundary conditions

against thermal expansion. In such case as mentioned in Eq. (18), a uniaxial type of buckling exists since the edges $y = \pm b/2$ are free to expand. As seen from Eq. (18), the compressive thermally induced force along the x direction is much lower than the one observed in biaxial thermal buckling. Consequently, it is expected that critical buckling temperatures for such plates are higher than those subjected to biaxial thermal loading. For this reason, a thin plate with $b/h = 50$ is considered and four different types of boundary conditions are examined. Five different aspect ratios are considered and as expected with increasing the plate length, critical buckling temperature decreases. A comparison among the results of Tables 8 and 9 reveals that, critical buckling temperature of thermally loaded SFSF plates are even higher than SSSS plates subjected to biaxial thermal compression. As an interesting result, it is observed that, critical buckling temperature of SXSX and CFXF are close to each other and approximately are equal. However, as expected the thermally buckled pattern for these two cases of boundary conditions are completely different.

Figure 2 demonstrates the thermally buckled pattern of FG-CNTRC plates with various boundary conditions, CNT volume fraction $V^*_{CN} = 0.12$, FG-X pattern of CNTs, $a/h = 50$ and $a/b = 2$. In this figure both uniaxially and biaxially loaded plates are depicted. Again, it is observed that, essential conditions are satisfied at the edges. Unlike the CCCC plate examined in Fig. 1, it is seen that buckling pattern of the plate is double symmetric. Such feature is expected since aspect ratio is of the main factors in buckled pattern of the rectangular plates.

5 Conclusion

Based on the first order shear deformation theory of plates, thermal buckling response of carbon nanotube reinforced rectangular plates is investigated in this research. Properties of the CNTs and the polymeric matrix are assumed to be temperature dependent. Only the case of uniform temperature rise parameter is considered. Distribution of CNTs across the plate thickness may be uniform or functionally graded. To obtain the thermomechanical properties of the composite plate, a refined rule of mixtures approach is developed to capture the size dependent features of CNTs. A Ritz solution with the Chebyshev basis shape functions suitable for arbitrary boundary conditions is implemented to construct the eigenvalue problem associated with the critical buckling temperature and buckled shapes of the plate. Numerical examples cover the influences of volume fraction of CNTs, dispersion pattern of CNTs, boundary conditions, plate aspect ratio and width to thickness ratio. It is shown that, in all of the studied cases, FG-X distribution of CNTs is the most efficient type for thermal buckling analysis since under such distribution, critical buckling temperature is higher in comparison to the other types of distribution of CNTs. Furthermore it is shown that, in-plane and out-of-plane boundary conditions, aspect ratio, side to thickness ratio and CNT volume fraction are all influential on critical buckling temperature as well as buckled pattern of the plate.

References

1. Kiani Y, Bagherizadeh E, Eslami MR (2011) Thermal buckling of clamped thin rectangular FGM plates resting on Pasternak elastic foundation (three approximate analytical solutions). ZAMM 91:581–593
2. Bateni M, Kiani Y, Eslami MR (2013) A comprehensive study on stability of FGM plates. Int J Mech Sci 75:134–144
3. Zhao X, Lee YY, Liew KM (2009) Mechanical and thermal buckling analysis of functionally graded plates. Compos Struct 90:161–171
4. Zhang LW, Zhu P, Liew KM (2014) Thermal buckling of functionally graded plates using a local Kriging meshless method. Compos Struct 108:472–492
5. Na KS, Kim JH (2004) Three-dimensional thermal buckling analysis of functionally graded materials. Compos B Eng 35:429–437
6. Zhu P, Zhang LW, Liew KM (2014) Geometrically nonlinear thermomechanical analysis of moderately thick functionally graded plates using a local Petrov Galerkin approach with moving Kriging interpolation. Compos Struct 107:298–314
7. Shen HS (2007) Thermal postbuckling behavior of shear deformable FGM plates with temperature-dependent properties. Int J Mech Sci 49:466–478
8. Zhang DG, Zhou HM (2015) Mechanical and thermal postbuckling analysis of FGM rectangular plates with various supported boundaries resting on nonlinear elastic foundations. Thin Walled Struct 89:142–151
9. Kiani Y, Esami MR (2012) Thermal buckling and postbuckling response of imperfect temperature-dependent

sandwich FGM plates resting on elastic foundation. Arch Appl Mech 82:891–905
10. Prakash T, Singha MK, Ganapathi M (2009) Thermal snapping of functionally graded materials plates. Mater Des 30:4532–4536
11. Liew KM, Yang J, Kitipornchai S (2004) Thermal post-buckling of laminated plates comprising functionally graded materials with temperature-dependent properties. J Appl Mech 71:839–850
12. Park JS, Kim JH (2006) Thermal postbuckling and vibration analyses of functionally graded plates. J Sound Vib 289:77–93
13. Liew KM, Lei ZX, Zhang LW (2015) Mechanical analysis of functionally graded carbon nanotube reinforced composites: a review. Compos Struct 120:90–97
14. Kwon H, Bradbury CR, Leparoux M (2013) Fabrication of functionally graded carbon nanotube-reinforced aluminum matrix composite. Adv Eng Mater 13:325–329
15. Shen HS (2009) Nonlinear bending of functionally graded carbon nanotube reinforced composite plates in thermal environments. Compos Struct 91:9–19
16. Jafari MS, Sobhani AB, Khoshkhahesh V, Taherpour A (2012) Mechanical buckling of nanocomposite rectangular plate reinforced by aligned and straight single walled carbon nanotubes. Compos B Eng 43:2031–2040
17. Lei ZX, Zhang LW, Liew KM (2013) Buckling analysis of functionally graded carbon nanotube-reinforced composite plates using the element-free kp-Ritz method. Compos Struct 98:160–168
18. Zhang LW, Lei ZX, Liew KM (2015) An element-free IMLS-Ritz framework for buckling analysis of FG-CNT reinforced composite thick plates resting on Winkler foundations. Eng Anal Bound Elem 58:7–17
19. Lei ZX, Zhang LW, Liew KM (2015) Buckling of FG-CNT reinforced composite thick skew plates resting on Pasternak foundations based on an element-free approach. Appl Math Comput 266:773–791
20. Zhang LW, Lei ZX, Liew KM (2015) Buckling analysis of FG-CNT reinforced composite thick skew plates using an element-free approach. Compos B Eng 75:36–46
21. Wu CP, Chang SK (2014) Stability of carbon nanotube-reinforced composite plates with surface-bonded piezoelectric layers and under bi-axial compression. Compos Struct 111:587–601
22. Shen HS, Zhu ZH (2012) Postbuckling of sandwich plates with nanotube-reinforced composite face sheets resting on elastic foundations. Eur J Mech A Solids 35:10–21
23. Shen HS, Zhang CL (2010) Thermal buckling and post-buckling behavior of functionally graded carbon nanotube-reinforced composite plates. Mater Des 31:3403–3411
24. Zhang LW, Liew KM, Reddy JN (2016) Postbuckling of carbon nanotube reinforced functionally graded plates with edges elastically restrained against translation and rotation under axial compression. Comput Methods Appl Mech Eng 298:1–28
25. Rafiee M, He XQ, Mareishi S, Liew KM (2015) Nonlinear response of piezoelectric nanocomposite plates: large deflection, post-buckling and large amplitude vibration. Int J Appl Mech 7:1550074 (32 pages)
26. Zhang LW, Lei ZX, Liew KM, Yu JL (2014) Large deflection geometrically nonlinear analysis of carbon nanotube-reinforced functionally graded cylindrical panels. Comput Methods Appl Mech Eng 273:1–18
27. Zhang LW, Liew KM (2015) Large deflection analysis of FG-CNT reinforced composite skew plates resting on Pasternak foundations using an element-free approach. Compos Struct 132:974–983
28. Zhang LW, Song ZG, Liew KM (2015) Nonlinear bending analysis of FG-CNT reinforced composite thick plates resting on Pasternak foundations using the element-free IMLS-Ritz method. Compos Struct 128:165–175
29. Zhang LW, Liew KM (2015) Geometrically nonlinear large deformation analysis of functionally graded carbon nanotube reinforced composite straight-sided quadrilateral plates. Comput Methods Appl Mech Eng 295:219–239
30. Zhang LW, Lei ZX, Liew KM (2015) Vibration characteristic of moderately thick functionally graded carbon nanotube reinforced composite skew plates. Compos Struct 122:172–183
31. Zhang LW, Lei ZX, Liew KM (2015) Free vibration analysis of functionally graded carbon nanotube-reinforced composite triangular plates using the FSDT and element-free IMLS-Ritz method. Compos Struct 120:189–199
32. Zhang LW, Lei ZX, Liew KM, Yu JL (2014) Static and dynamic of carbon nanotube reinforced functionally graded cylindrical panels. Compos Struct 111:205–212
33. Zhang LW, Song ZG, Liew KM (2015) State-space Levy method for vibration analysis of FG-CNT composite plates subjected to in-plane loads based on higher-order shear deformation theory. Compos Struct 134:989–1003
34. Zhang LW, Cui WC, Liew KM (2015) Vibration analysis of functionally graded carbon nanotube reinforced composite thick plates with elastically restrained edges. Int J Mech Sci 103:9–21
35. Lei ZX, Zhang LW, Liew KM (2015) Free vibration analysis of laminated FG-CNT reinforced composite rectangular plates using the kp-Ritz method. Compos Struct 127:245–259
36. Zhang LW, Lei ZX, Liew KM (2015) Computation of vibration solution for functionally graded carbon nanotube-reinforced composite thick plates resting on elastic foundations using the element-free IMLS-Ritz method. Appl Math Comput 256:488–504
37. Lei ZX, Zhang LW, Liew KM (2015) Elastodynamic analysis of carbon nanotube-reinforced functionally graded plates. Int J Mech Sci 99:208–217
38. Lei ZX, Zhang LW, Liew KM, Yu JL (2014) Dynamic stability analysis of carbon nanotube-reinforced functionally graded cylindrical panels using the element-free kp-Ritz method. Compos Struct 113:328–338
39. Malekzadeh P, Heydarpour Y (2015) Mixed Navier-layerwise differential quadrature three-dimensional static and free vibration analysis of functionally graded carbon nanotube reinforced composite laminated plates. Meccanica 50:143–167
40. Alibeigloo A, Emtehani A (2015) Static and free vibration analyses of carbon nanotube-reinforced composite plate using differential quadrature method. Meccanica 50:61–67
41. Shi DL, Feng XQ, Huang YY, Hwang KC, Gao HJ (2004) The effect of nanotube waviness and agglomeration on the elastic property of carbon nanotube reinforced composites. J Eng Mater Technol 126:250–257

42. Fidelus JD, Wiesel E, Gojny FH, Schulte K, Wagner HD (2005) Thermo-mechanical properties of randomly oriented carbon/epoxy nanocomposites. Compos A Appl Sci Manuf 36:1555–1561
43. Shen HS (2011) Postbuckling of nanotube-reinforced composite cylindrical shells in thermal environments, part I: axially-loaded shells. Compos Struct 93:2096–2108
44. Jam JE, Kiani Y (2015) Buckling of pressurized functionally graded carbon nanotube reinforced conical shells. Compos Struct 125:586–595
45. Jam JE, Kiani Y (2015) Low velocity impact response of functionally graded carbon nanotube reinforced composite beams in thermal environment. Compos Struct 132:35–43
46. Mirzaei M, Kiani Y (2015) Snap-through phenomenon in a thermally postbuckled temperature dependent sandwich beam with FG-CNTRC face sheets. Compos Struct 134: 1004–1013
47. Mirzaei M, Kiani Y (2015) Thermal buckling of temperature dependent FG-CNT reinforced composite conical shells. Aerosp Sci Technol 47:42–53
48. Reddy JN (2003) Mechanics of laminated composite plates and shells, theory and application. CRC Press, Boca Raton
49. Wang ZX, Shen HS (2011) Nonlinear vibration of nanotube-reinforced composite plates in thermal environments. Comput Mater Sci 50:2319–2330
50. Jones RM (2005) Thermal buckling of uniformly heated unidirectional and symmetric cross-ply laminated fiber-reinforced composite uniaxial in-plane restrained simply supported rectangular plates. Compos A 36:1355–1367
51. Shen HS, Xiang Y (2013) Nonlinear analysis of nanotube-reinforced composite beams resting on elastic foundations in thermal environments. Eng Struct 56:698–708
52. Han Y, Elliott J (2007) Molecular dynamics simulations of the elastic properties of polymer/carbon nanotube composites. Comput Mater Sci 39:315–323
53. Wang CY, Zhang LC (2008) A critical assessment of the elastic properties and effective wall thickness of single-walled carbon nanotubes. Nanotechnology 19:075705
54. Shen HS (1998) Thermal postbuckling analysis of imperfect Reissner- Mindlin plates on softening nonlinear elastic foundations. J Eng Math 33:259–270
55. Matsunaga H (2005) Thermal buckling of cross-ply laminated composite and sandwich plates according to a global higher-order deformation theory. Compos Struct 68:439–454
56. Noor AK, Burton WS (1992) Three-dimensional solutions for thermal buckling of multilayered anisotropic plates. J Eng Mech 118:683–701
57. Singh S, Singh J, Shukla K (2013) Buckling of laminated composite plates subjected to mechanical and thermal loads using meshless collocations. J Mech Sci Technol 27:327–336